Eur. Phys. J. D **39**, 209–221 (2006)
DOI: 10.1140/epjd/e2006-00088-0

THE EUROPEAN PHYSICAL JOURNAL D

Primary electron spectra from swift heavy-ion impact

Scaling relations and estimates from modified Bohr theory

M.S. Weng[1,a], A. Schinner[2], A. Sharma[1,b], and P. Sigmund[1,c]

[1] Physics Department, University of Southern Denmark, 5230 Odense M, Denmark
[2] Institut für Experimentalphysik, Johannes-Kepler-Universität, 4040 Linz-Auhof, Austria

Received 18 January 2006 / Received in final form 6 March 2006
Published online 20 April 2006 –

Abstract. We have calculated single-differential energy spectra of electrons emitted in swift-ion-atom collisions on the basis of the classical Bohr theory allowing for various extensions. Special emphasis has been paid to scaling relationships which are inherent in the Bohr theory but would not emerge from simple Coulomb scattering or conventional binary-encounter theory. We consider electrons emitted from the target as well as the projectile. In addition to electron binding, which is known to be treated well in the Bohr theory, we allow for orbital motion of target and projectile electrons and apply a feasible description of the screened interaction of partially-stripped projectile ions. Predicted scaling laws as well as absolute estimates are compared with experimental data.

PACS. 34.50.Fa Electronic excitation and ionization of atoms (including beam-foil excitation and ionization) – 52.20.Hv Atomic, molecular, ion, and heavy-particle collisions – 79.20.Rf Atomic, molecular, and ion beam impact and interactions with surfaces

1 Introduction

The phenomenon of ionization in ion-atom collisions is closely related to the associated energy loss by the colliding ion. Indeed, most of the energy loss suffered by a swift ion in the collision with an atom at rest goes into the energy of emitted electrons, except in very soft interactions. In Bohr's classical treatise [1], careful distinction was made between energy loss and ionization, yet the two phenomena were treated in parallel throughout the pertinent chapters.

With the increasing sophistication of experimental and theoretical techniques, and a general trend toward specialization, awareness of this close connection has decreased continuously, and very little use has been made of developments in one field to provoke progress in the other. This striking feature becomes immediately evident from inspection of recent reviews, both of electron emission [2,3] and particle stopping [4–6].

The present study has been stimulated by recent progress in the field of particle stopping, specifically the stopping of swift, partially stripped heavy ions in matter. While we do by no means have the ambition to compete with highly sophisticated and quite successful theoretical treatments of doubly-differential spectra of emitted electrons, we have some quite specific points in mind:

- any theory of particle stopping contains — implicitly or explicitly — a model for excited-electron spectra. Explicit determination of such spectra and proper comparison with experimental electron spectra provides a more stringent test on stopping theory than a mere comparison of stopping cross-sections;
- systematic use of scaling relations, i.e., plotting physical quantities in terms of 'natural' variables is a well-established technique in stopping theory. Not only does this allow to test one's understanding, even more important, it is a very useful tool for interpolation between experimental and/or theoretical data. We found surprisingly little use of this technique in reported electron spectra going beyond fairly simplistic comparisons on the basis of Rutherford scattering;
- in radiation physics, especially the field of particle tracks, information is needed both on energy loss and energy spectra of liberated electrons. Input data for Monte Carlo simulations are extracted from theory. It is obviously desirable that the same theoretical scheme serve as the pertinent source;
- the needs of radiation physics point in the direction of a large number of combinations of projectiles and target materials of potential interest, while requirements on accuracy are modest. The trend in atomic-collision

[a] *Present address*: Vestfyns Gymnasium, 5620 Glamsbjerg, Denmark.
[b] *Present address*: Physics Department, Kurukshetra University, 136 119 Kurukshetra, India.
[c] e-mail: psi@dou.dk

physics — driving in the direction of full understanding of the dominating processes — is opposite, favoring few collision systems and high accuracy;
– most detailed information in ion-atom collisions is achieved by studying doubly-differential angle-energy distributions of emitted electrons. Conversely, for collisions in dense material, angular distributions are of little intrinsic interest because of frequent angular deflection of liberated electrons during slowing-down.

A common feature of the two considered fields is the fact that dependent on ion-target combination and beam velocity, successful theoretical treatments can be based either on the Born approximation or one of its descendents, or on some kind of classical-orbit theory. There has been full awareness of the complementary regimes of validity of these approaches, briefly expressed by the Bohr-Sommerfeld parameter $\kappa_{\rm Bohr} = 2Z_1 v_0/v$, where Z_1 is the atomic number of the ion, v its speed and $v_0 = c/137$ the Bohr speed. According to Bohr [1], the classical regime is specified by $\kappa_{\rm Bohr} \gg 1$, and the Born regime by $\kappa_{\rm Bohr} \ll 1$, and in practice there is an overlap regime described by either scheme with tolerable accuracy.

Our focus is on heavy ions, $Z_1 \gg 1$, i.e., primarily the classical regime at not too high beam speeds. In existing treatments of electron spectra, classical arguments enter at various stages of sophistication,

– straight Rutherford scattering,
– binary-encounter theory, i.e. Coulomb scattering taking into account orbital motion of target electrons, and
– classical-trajectory Monte Carlo computation.

Actually, only one of these tools makes explicit use of classical electron orbits.

In the field of particle stopping, the dominance of the Born approximation over classical-orbit arguments has been very strong for a long period, ever since the appearance of Bethe's classic paper [7], and it is only during the past decade that the original Bohr theory [8] has received attention again [9,10] and that Bloch's scheme, which incorporates Bethe and Bohr theory [11] has been rederived in a very transparent way and placed into context [12]. As a consequence, theory of heavy-ion stopping based on classical-orbit concepts has developed substantially [5].

A prime feature of Bohr stopping theory is a rather realistic model for binding of target electrons. While based on Drude-Lorentz electron theory, it actually survived the advent of quantum mechanics with a moderate adjustment. Scaling properties implied by this model do not simply emerge from Rutherford scattering or the binary-encounter model. A substantial fraction of this paper will be devoted to such scaling relations and to testing their validity against both experimental data and theoretical calculations.

Processes contributing to electron emission are well known and well categorized [13,2,3]. Within the chosen scope of this paper we must admit from the beginning that there are several that we cannot treat. There is no way to treat Auger electrons in a classical scheme, nor can we treat electron capture into the continuum. However we can treat quasi-binary ion-electron interactions over a very wide range of momentum transfers, taking due account of orbital motion and binding forces, we can do the same for projectile electrons emitted by collisions with the target nucleus, and we have a way to describe partially-ionized projectiles that is far more realistic than conventional effective-charge models.

Our main theoretical tool is what we call binary stopping theory [14,15], which we ask the reader not to mix up with binary-encounter collision theory. Binary theory is an expansion of the Bohr theory which, first of all, takes into account the difference between particles and antiparticles as projectiles, i.e., gives rise to terms uneven in Z_1, called Barkas-Andersen terms in stopping theory. However, scaling relations predicted by binary theory follow largely from the Bohr model. Therefore, considerable space will be devoted to a thorough study of the implications of the Bohr model. We emphasize that Bohr himself, in his 1948 review [1], refrained from exploring these properties.

This project dates back to the M.Sc. thesis of one of us [16], who calculated differential and integral ionization cross-sections from Bohr theory. Results were found promising enough to be presented orally at a conference on particle tracks[1]. A simultaneous attempt to apply binary theory was less successful because the PASS code implementing binary theory needed substantial modification before allowing to compute emitted-electron spectra. This had been achieved in 2004, where a poster was presented by the present group of authors [17]. Special attention was, however, required to the treatment of projectile processes which have only recently been incorporated into the PASS code. Therefore, this is the first submitted paper reporting our efforts in the area over five years.

2 Bohr theory

2.1 Bare ion on single-shell atom

2.1.1 Energy transfer

Bohr's original theory [8] deals with the energy transfer $T(v,p)$ from a point charge in uniform motion to a single classical electron, bound harmonically to a stationary nucleus with an oscillator frequency ω and initially at rest. Here, v is the projectile speed and p the impact parameter. Bohr divided up the range of impact parameters into regimes of close and distant interactions, where close collisions obey the Thomson formula for free-Coulomb scattering. Distant interactions, on the other hand, are characterized as dipole excitations known from Drude-Lorentz electron theory. From the asymptotic behavior at large arguments, Bohr deduced that the effective interaction potential is screened to within the adiabatic distance

$$a_{\rm ad} = \frac{v}{\omega}. \tag{1}$$

[1] EUNITT workshop, February 2002 in Caen.

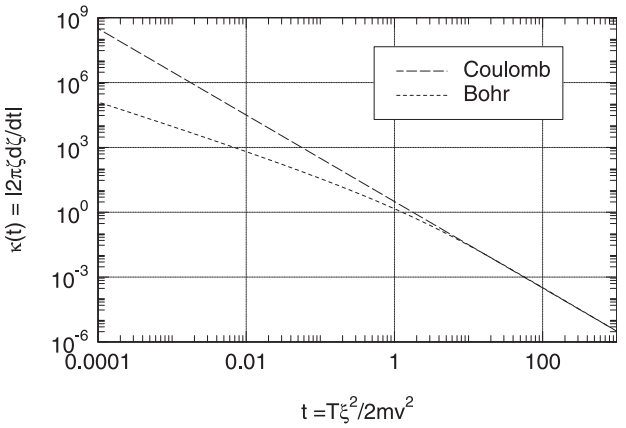

Fig. 1. Differential energy-transfer cross-section in dimensionless units for a bare ion interacting with a harmonically bound target electron. Dotted line: Bohr model; dashed line: free-Coulomb scattering.

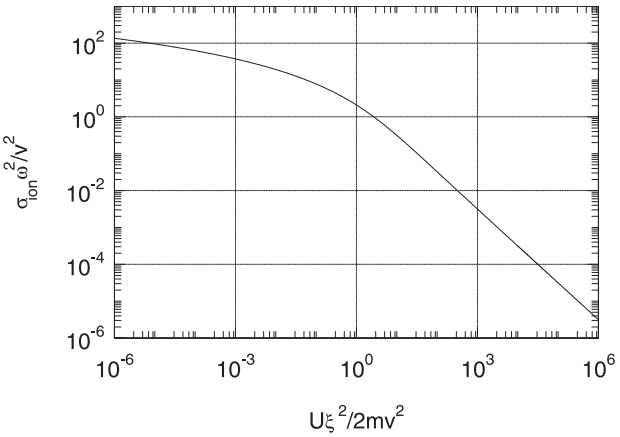

Fig. 2. Universal plot of the ionization cross-section of a single-shell atom for a bare projectile ion in dimensionless units for beam energies far above threshold. Bohr model.

After introduction of dimensionless variables for impact parameter, energy transfer and velocity,

$$\zeta = \frac{\omega p}{v} \tag{2a}$$

$$t = \frac{T\xi^2}{2mv^2} \tag{2b}$$

$$\xi = \frac{mv^3}{Z_1 e^2 \omega}. \tag{2c}$$

we may summarize the Bohr model in the scaled form

$$t = \frac{1}{\zeta^2 + 1/\xi^2} \quad \text{(close)} \tag{3a}$$

$$t = [K_1(\zeta)]^2 + [K_0(\zeta)]^2 \quad \text{(distant)}. \tag{3b}$$

2.1.2 Differential cross-section

The differential cross-section for energy transfer (T, dT) reads, in dimensionless units,

$$\kappa(t) = \left| \frac{2\pi\zeta}{dt/d\zeta} \right|. \tag{4}$$

It is readily seen from equation (3) that the dimensionless velocity variable ξ drops out after differentiation, and that the differential cross-section reduces to a universal curve independent of ξ, which is shown in Figure 1.

It is seen that unlike in the energy transfer, equation (3), it is not necessary to split collisions into close and distant interactions, since the differential cross-section derived from the Bohr formula (Eq. (3)) actually coincides with the free-Coulomb cross-section at high t, i.e., in the latter's domain of validity.

Note that the maximum energy transfer $T_{\max} = 2mv^2$ corresponds to $t_{\max} = \xi^2$ at a given projectile speed according to equation (2). Evidently, even though the differential cross-section obeys a universal scaling law in this approximation, the actual cross-section at a given value of v or ξ is truncated.

We also may deduce from Figure 1 that significant deviations from free-Coulomb scattering must be expected for $T \lesssim 2mv^2/\xi^2$.

We may convert the energy-loss cross-section into a differential ionization cross-section $d\sigma(\epsilon)/d\epsilon$ by substituting

$$\epsilon = T - U, \tag{5}$$

where ϵ is the energy of a liberated electron and U its binding energy.

2.1.3 Total ionization cross-section

For $2mv^2 \gg U$, the total ionization cross-section $\sigma_{\rm ion} = \int_U^{2mv^2} d\sigma(T)$ may be approximated by $\sigma_{\rm ion} \simeq \pi p_c^2$ for $2mv^2 \gg U$, where p_c is the impact parameter at which $T = U$. This assumes the energy transfer T to be a monotonically decreasing function of p. In dimensionless units this reads

$$\frac{\omega^2}{v^2}\sigma_{\rm ion} \simeq \pi\zeta_c^2, \tag{6}$$

where ζ_c is a universal function of $U\xi^2/2mv^2$ shown in Figure 2.

Significant deviations occur from the scaling behavior indicated by Figure 2 in the threshold regime where $2mv^2$ comes close to U.

2.1.4 Scaling

From equation (2) and Figure 1 we may deduce that in the Bohr model, the proper dimensionless measure of the energy loss is the quantity

$$t = \frac{T\xi^2}{2mv^2} = \frac{2mv^2 T}{(\hbar\omega\kappa_{\rm Bohr})^2}, \tag{7}$$

where $\kappa_{\rm Bohr} = 2Z_1 e^2/\hbar v$ is $\gg 1$ in the classical regime.

The corresponding variable in the Born approximation can be found e.g. by considering the scattering from a Yukawa potential with the screening radius $a_{\rm ad}$ defined by equation (1),

$$d\sigma(T) = \pi \left(\frac{2Z_1 e^2}{\hbar\omega}\right)^2 \frac{du}{(u+1)^2} \tag{8}$$

with the scaling variable

$$u = \frac{2mv^2 T}{(\hbar\omega)^2}, \tag{9}$$

i.e., the limit of equation (7) for $\kappa_{\rm Bohr} = 1$. This ensures a continuous transition from the classical to the Born regime.

2.2 Dressed ion on single-shell atom

2.2.1 Energy transfer

When the projectile ion carries electrons, its interaction with the target electrons may be approximated by a screened Coulomb potential. In reference [10], an *ansatz*

$$V(r) = -\frac{q_1 e^2}{r} - \frac{(Z_1 - q_1)e^2}{r} e^{-r/a_{\rm sc}} \tag{10}$$

was employed, where q_1 is the charge state of the ion. The general form of this relation was suggested by Brandt and Kitagawa [18], but the screening radius $a_{\rm sc}$ was taken in [10] as $a_{\rm sc} = (1 - q_1/Z_1)\, a_{\rm TF}$ where $a_{\rm TF} = 0.8853 a_0/Z_1^{1/3}$ is the Thomas-Fermi radius of a neutral projectile. This expression was found on the basis of the Fermi-Amaldi model of atomic ions. The classical energy loss can be calculated in the dipole approximation and reads [10]

$$T(v,p) = \frac{2Z_1^2 e^4 \omega^2}{mv^4} \left\{ \Big[\beta K_0(\zeta) + (1-\beta) K_0(\alpha\zeta)\Big]^2 + \Big[\beta K_1(\zeta) + (1-\beta)\alpha K_1(\alpha\zeta)\Big]^2 \right\}, \tag{11}$$

where $\beta = q_1/Z_1$ is the degree of ionization and

$$\alpha = \sqrt{1 + \left(\frac{a_{\rm ad}}{a_{\rm sc}}\right)^2}. \tag{12}$$

Screening by projectile electrons affects mostly distant collisions. The influence on close collisions will be seen in connection with binary theory.

Figure 3 shows an example for $\beta = q_1/Z_1 = 2/3$. It is seen that at large impact parameters, where only the first term in the brackets in equation (11) is significant, curves for different values of ξ merge and lie a factor of $\beta^2 = 4/9$ below the curve for the bare ion. All curves merge for small impact parameters, as they have to with the chosen ordinate variable. Deviations at intermediate impact parameters reflect the different values of $a_{\rm ad}/a_{\rm sc}$.

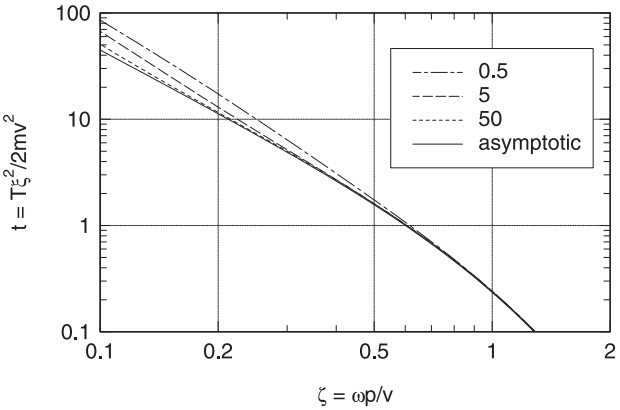

Fig. 3. Scaled energy loss $t = T\xi^2/2mv^2$ versus scaled impact parameter $\zeta = \omega p/v$ for charge ratio $\beta = q_1/Z_1 = 2/3$ in the Bohr model, distant collisions. Curves for $\xi = 0.5, 5$ and 50 calculated from equation (11). The curve labelled 'asymptotic' represents the energy loss of a point charge $q_1 = \beta Z_1$.

2.2.2 Differential cross-section

Figure 4 shows differential cross-sections corresponding to the dotted curve in Figure 1 for charge ratios $\beta = q_1/Z_1 = 2/3, 1/3$ and 0, all of them being compared with that for $\beta = 1$ from Figure 1. As follows from equation (11), the simple scaling is broken, so curves for different ξ do not any longer coincide at a fixed charge ratio. Nevertheless, scaling is still approximately valid for $q_1/Z_1 = 2/3$ at all t, and for $q_1/Z_2 = 1/3$ at least for $t \gtrsim 0.1$.

3 Binary theory

3.1 Binding versus screening

The essential feature in binary stopping theory is the replacement of a binding force by a screening function in the potential. This is an appealing replacement, since the pertinent quantity for stopping is the energy transfer versus impact parameter, $T(p)$, and since both binding and screening have the effect of reducing $T(p)$ below the Coulomb value at large impact parameters. Well-established procedures are available for the solution of binary scattering problems on a screened potential. Therefore, the problem is reduced to finding an appropriate screening potential as a realistic representation of the binding force. Lindhard [19] used this view in his analysis of the Z_1^3 correction to Bethe's stopping formula. In reference [14], two of us have demonstrated that the equivalence of the two views is even more fargoing.

3.2 Bare ion on single-shell atom

3.2.1 Energy transfer

Following reference [19], the ion-electron Coulomb interaction is characterized by a Yukawa potential

$$V(r) = -\frac{Z_1 e^2}{r} e^{-r/a_{\rm ad}}. \tag{13}$$

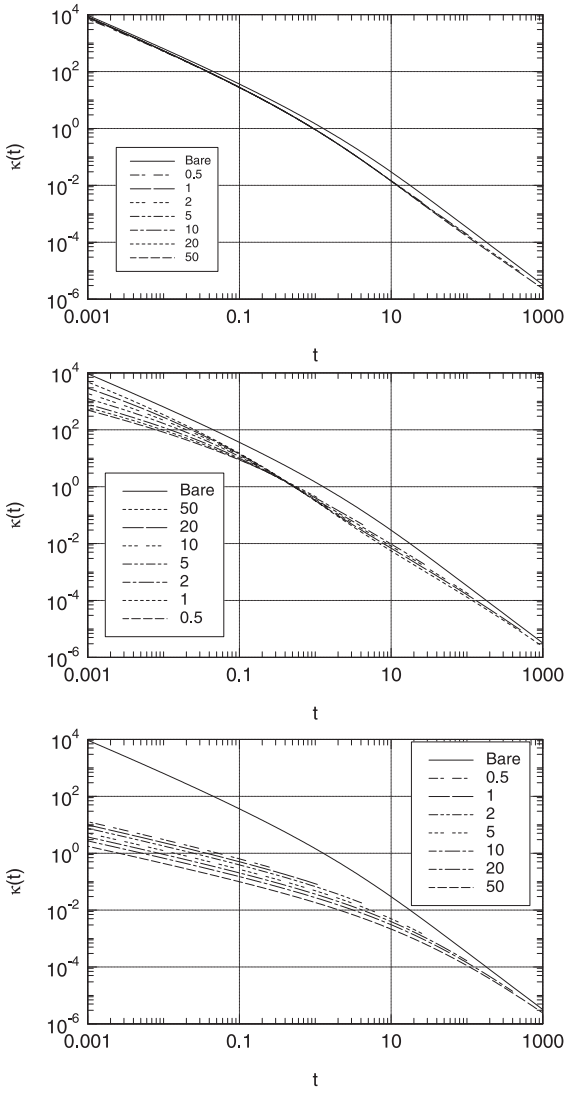

Fig. 4. Same as Figure 1 but for dressed instead of bare ion, according to equation (11). Charge fractions $\beta = q_1/Z_1 = 2/3, 1/3, 0$ (top to bottom). Labels indicate the value of the velocity measure $\xi = mv^3/Z_1e^2\omega$. The curve labeled 'Bare' is the dotted curve from Figure 1.

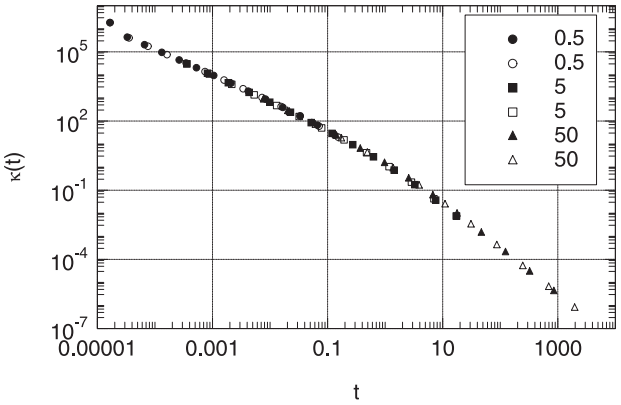

Fig. 5. Differential cross-sections per target electron, calculated from binary theory for bare carbon and anticarbon ions on helium, plotted in dimensionless units, equation (2) for $\xi = 0.5, 5$ and 50. For clarity only few points are included. Filled symbols: carbon; empty symbols: anticarbon.

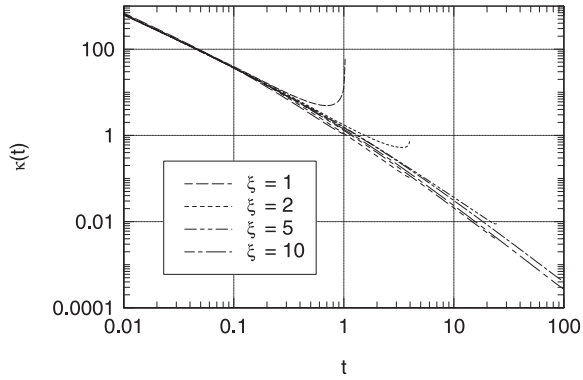

Fig. 6. Same as Figure 5 for $\xi = 1, 2, 5$ and 10. Thin lines: bare carbon ions on helium; thick lines: anticarbon ions on helium.

It was demonstrated in reference [14] that classical scattering theory with the potential (13) rigorously reproduces the first term in equation (3) at large impact parameters. This term represents the energy transfer perpendicular to the beam, i.e., the transverse momentum transfer which dominates in distant collisions.

The second term in the brackets of equation (3) represents longitudinal momentum transfer. This term does not emerge directly from binary scattering theory. In reference [14] it was interpreted as a potential-energy transfer related to the angular momentum achieved by a target electron in a collision. While there is no potential-energy transfer in a free binary collision, the electron does achieve angular momentum in the laboratory frame of reference, and that angular momentum can be determined from scattering theory via the so-called time integral. In this manner, the potential-energy term was likewise reproduced rigorously from classical scattering theory.

Since both binding and screening become insignificant at small impact parameters, results from binary scattering theory extrapolate toward free-Coulomb scattering for close collisions. Successful tests were also performed on intermediate impact parameters by comparison with Z_1^3-terms in the Bohr theory.

3.2.2 Differential cross-section

Figure 5 shows differential cross-sections calculated from binary theory for bare carbon and anticarbon ions for a wide range of ξ-values. Comparison with Figure 1 shows that the scaling properties implied by the Bohr model are very well fulfilled at least on the scale of the graph.

Figure 6 shows the same information on a finer scale. Two kinds of deviation from universal scaling are observed:

1. there is a difference between carbon and anticarbon ions for close collisions. In the field of particle stopping,

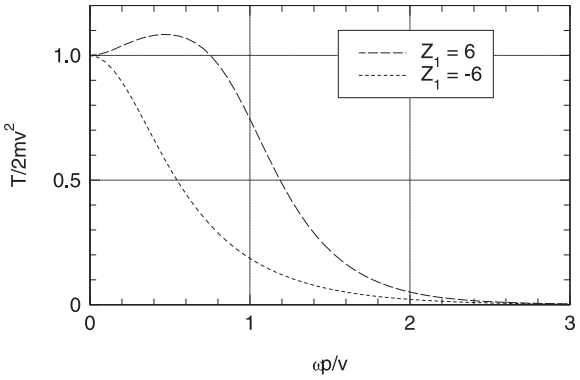

Fig. 7. Energy loss per target electron versus impact parameter calculated from binary theory excluding (shell correction) for C–He and $\xi = 1$. The curve labeled '$Z_1 = -6$' denotes anti-carbon.

this is called the Barkas or Barkas-Andersen effect. The magnitude of this difference in the mean energy loss, as calculated from binary stopping theory, has been shown to be in very good agreement with measurements down to beam velocities well below v_0 [20];

2. at low projectile speeds, for $\xi = 1$ and 2 in Figure 6, peaks at the maximum energy transfer are observed. The origin of this feature is illustrated in Figure 7: for positive carbon ions, the energy loss initially increases with increasing impact parameter and goes through a maximum before decreasing monotonically. In the binary theory, this effect enters through the potential-energy contribution which is expressed by the angular-momentum transfer which vanishes at zero impact parameter.
While we do not know the accuracy with which this effect is described in the binary theory, we have no reason to doubt its existence. Similar observations have been made by Basko [21] in numerical simulations of the genuine Bohr model.
While the effect will be smeared out by the shell correction to be discussed below, we need to keep in mind that here is a possible source of error for the case of hard collisions at beam velocities corresponding to $\xi \lesssim 2$.

3.3 Dressed ion on single-shell atom

3.3.1 Energy transfer

Incorporation of static screening of the projectile into binary stopping theory follows the procedure outlined in the previous section, except that it is scattering on the potential (10) that is to be modeled instead of a bare-Coulomb potential. Correspondingly, the criterium of validity of the procedure is quantitative reproduction of equation (11) for distant collisions. The key to a valid description is a correct combination of static and dynamic screening. This is achieved by the potential

$$V(r) = -\frac{q_1 e^2}{r} e^{-r/a_{\mathrm{ad}}} - \frac{(Z_1 - q_1)e^2}{r} e^{-r/a}, \qquad (14)$$

where

$$\frac{1}{a^2} = \frac{1}{a_{\mathrm{ad}^2}} + \frac{1}{a_{\mathrm{sc}}^2}, \qquad (15)$$

and a_{sc} is the static screening radius which depends on the charge state.

An explicit derivation of equation (11) from equation (14) by binary scattering theory has been given in [14]. As in case of the bare ion, this derivation involves both the scattering angle and the time integral.

3.3.2 Differential cross-section

Figure 8 shows differential cross-sections calculated from the simplest version of binary theory — excluding orbital motion and emission of projectile electrons — for C^{6+}, C^{4+}, C^{2+} and C^0 incident on He at three different beam energies. At the highest energy, 1.48 MeV/u, all cross-sections merge at large energy transfers, but significant differences are found for softer interactions. Conversely, at the lowest beam energy, 0.109 MeV/u, the charge state also affects close collisions.

Singular behavior near the maximum energy transfer gets increasingly pronounced for lower charge states. It is, however, restricted to a very narrow ϵ-interval.

Evidently, none of these dependencies can be characterized by q_1^2 scaling of the free-Coulomb cross-section. This is in complete accordance with our experience from stopping cross-sections [22] and equivalent experience in electron spectra [23].

4 Inclusion of orbital motion

4.1 Kinetic theory

In binary stopping theory, orbital motion of target and projectile electrons is treated as a transformation between moving reference frames in accordance with kinetic theory [24]. Although relativistic relationships are available [25], they have not been applied in practice because nonrelativistic relationships appear adequate in stopping theory. This may not necessarily be true in electron spectra, but we shall disregard this possibility here.

When applied to straight Coulomb scattering, kinetic theory produces results equivalent with binary-encounter theory [26], but the basic kinetic equations apply rigorously to any binary interaction potential and, as they stand, have proven successful in connection with bound electrons. A recent example of a surprisingly accurate approximation to an exact result has been given in reference [27].

The derivations in [24] are restricted to the first and second moment over the differential energy-loss cross-section, i.e., the stopping cross-section and the straggling

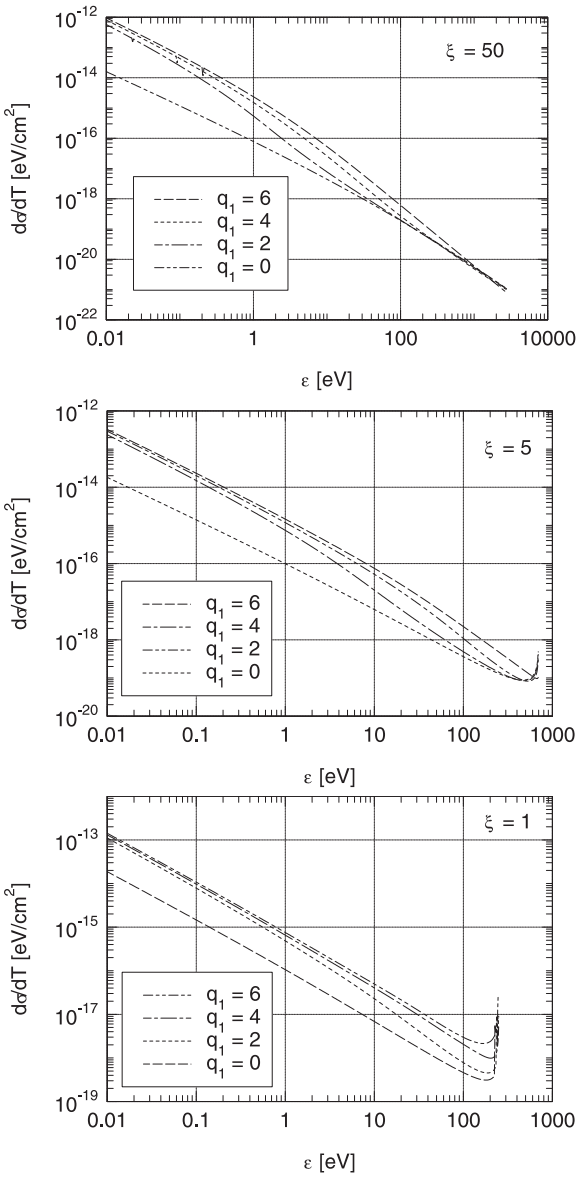

Fig. 8. Differential cross-sections calculated from binary theory excluding shell correction for C^{q_1+}–He at $\xi = 50$, 5, and 1, corresponding to ion energies 1.48, 0.319 and 0.109 MeV/u (top to bottom graph).

parameter. In the following we shall briefly describe the transformation of the differential cross-section itself. Separate attention needs to be paid to electrons emitted from the target and the projectile.

Note that these relations do not make explicit reference to binary stopping theory.

4.2 Transformation for target electrons

Consider the interaction between a projectile ion with a velocity $\boldsymbol{v}$ and a free electron with a velocity $\boldsymbol{v}_e$. In the notation of reference [24] the energy transferred to the electron can be expressed as $T = m\boldsymbol{v} \cdot (\boldsymbol{w}' - \boldsymbol{w})$, where

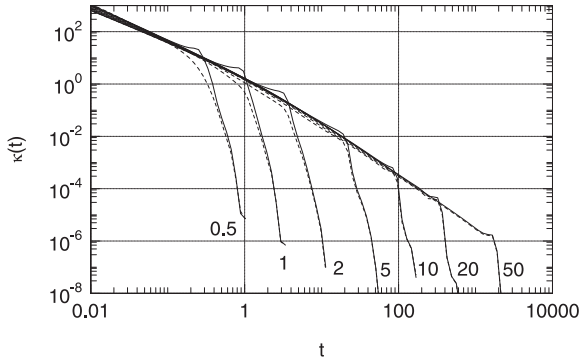

Fig. 9. Same as Figures 5 and 6 but including orbital motion of the target electrons. Solid lines: bare carbon ions; broken lines: anticarbon ions. Numbers denote the value of ξ.

$\boldsymbol{w} = \boldsymbol{v}_e - \boldsymbol{v}$ and $\boldsymbol{w}' = \boldsymbol{v}'_e - \boldsymbol{v}$ are the velocities of the target electron before and after the interaction in a reference frame moving with the projectile — i.e., the c.m.s. system.

For a velocity spectrum $g(\boldsymbol{v}_e)d^3v_e$, the contribution of those electrons to the differential cross-section for scattering over a c.m.s. angle θ is given by

$$d\sigma = \frac{w}{v} g(\boldsymbol{v}_e) d^3 v_e \, d\sigma_0(w, \theta), \tag{16}$$

where $d\sigma_0(v, \theta)$ is the differential cross-section for an initially stationary target electron, $\boldsymbol{v}_e = 0$.

With this, the differential energy-loss cross-section may be written as

$$\frac{d\sigma}{dT} = \left\langle \frac{w}{v} \int d\sigma_0(w, \theta) \, \delta\big[T - m\boldsymbol{v} \cdot (\boldsymbol{w}' - \boldsymbol{w})\big] \right\rangle, \tag{17}$$

where $\delta(\dots)$ indicates the Dirac function and the brackets an average over $\boldsymbol{v}_e$.

Evaluation in spherical coordinates leads to

$$\frac{d\sigma}{dT} = \frac{1}{\pi} \left\langle \frac{w}{v} \int \frac{d\sigma_0(w, \theta)}{\sqrt{D}} \right\rangle, \tag{18}$$

where

$$D = m^2 \left[w^2 v^2 - (\boldsymbol{v} \cdot \boldsymbol{w})^2 \right] \sin^2 \theta - \left[T + m\boldsymbol{v} \cdot \boldsymbol{w} (1 - \cos\theta) \right]^2. \tag{19}$$

4.3 Implementation

The remaining integration over d^3v_e assumes isotropy of the electron distribution. With this, two integrations remain. In [24], the most suitable integration variables were found to be v_e and w. An added subroutine to the PASS code implementing binary theory allows numerical integration of equation (18) for a given $d\sigma_0(w, \theta)$ and $g(v_e)$.

Figure 9 shows our standard example C–He at seven values of the velocity parameter ξ. The velocity spectrum $g(v_e)$ has been determined from hydrogenic wave functions with the charge adapted to the measured binding energy.

This procedure was also used to determine the majority of the velocity profiles underlying our tabulation of stopping force in reference [6]. As in Figures 5 and 6, data for bare carbon and for anticarbon ions have been included. As expected, a Barkas effect is seen in the close-collision region which, however, is vanishingly small at the highest velocity corresponding to $\xi = 50$.

5 Projectile electrons

All energy-loss cross-sections considered up to now may easily be converted into spectra of emitted electrons by means of the transformation (5) between the electron energy ϵ, energy loss T and binding energy U. This is not so in the process of electron emission from the projectile. Dependent on the desired amount of detail, this is a truly complex process, as has been amply demonstrated in the literature and summarized in reference [3].

5.1 The model

Bare of the ambition to describe angular spectra, we feel justified, as a first approximation, to ignore three- and four-body interactions in individual ion-atom collisions, i.e., events where an electron emitted from a target atom is deflected in the field of the projectile, and vice versa.

Moreover, we shall disregard binary collisions between target and projectile electrons, or antiscreening. This phenomenon is well established for collisions undergone by energetic neutral hydrogen beams, where the Coulomb interactions of the projectile nucleus and the projectile electron are equal. The effect becomes insignificant with increasing Z_1.

What remains is the possibility of excitation and emission of a projectile electron by the interaction with a target nucleus which is modeled as a screened nucleus with the total charge zero. The fact that the target atom is neutral and the projectile atom charged has the a priori consequence that projectile excitation rarely dominates, except for $Z_1 \gg Z_2$: the screened Coulomb force of the target atom tends to be weaker than that of a charged atom, and the number of electrons ready for emission from the projectile tends to be smaller from a charged projectile than from a neutral atom. Moreover, those projectile electrons tend to be more strongly bound.

In summary, emission of projectile electrons will be treated in as close analogy as possible with the emission of target electrons. The interaction potential will be given by equation (14) with $\beta = 0$, and the number of electrons on the projectile will be given by the charge state. However, care needs to be applied to proper transformation of the kinetic equations from the projectile frame to the laboratory frame of reference.

5.2 Stationary projectile electron

For orientation we first consider the case of negligible orbital motion of the projectile electron. Denoting variables

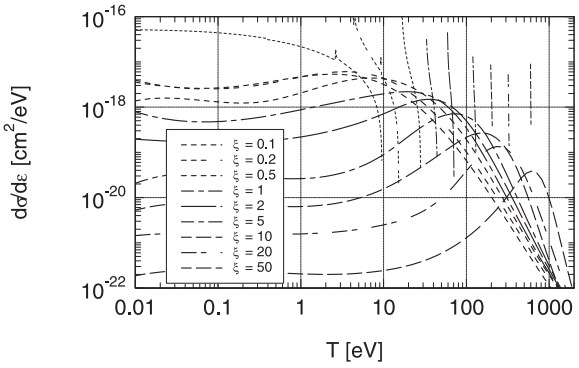

Fig. 10. Differential cross-section for electron emission from projectile for neutral helium incident on carbon. Thin lines: excluding orbital electron motion. Thick lines: including orbital motion.

in the reference frame $\mathcal{S}'$ moving with the projectile by primes, the energy of an emitted electron reads

$$\epsilon' = 2mv^2 \sin^2 \frac{\theta}{2} - U, \tag{20}$$

where θ is the c.m.s. scattering angle in a binary collision between the projectile electron and the screened (neutral) target nucleus.

The direction of motion of the electron after the collision is given by an angle $\phi' = (\pi - \theta)/2$. This defines the velocity vector, and after transformation back to the laboratory system we find the electron energy

$$\epsilon = \frac{m}{2}v^2 - U + 2mv^2 \sin^2 \frac{\theta}{2} - mv \sin \frac{\theta}{2} \sqrt{4v^2 \sin^2 \frac{\theta}{2} - 2U/m}. \tag{21}$$

We may write the differential cross-section in the form

$$d\sigma(\epsilon) = d\epsilon \int d\sigma(v,T) \times \delta\left(\epsilon - \frac{m}{2}v^2 + U - T + T\sqrt{1 - U/T}\right), \tag{22}$$

where $T = 2mv^2 \sin^2(\theta/2)$, and $d\sigma(v,T)$ the cross-section with the roles of ion and target interchanged.

Integration over T yields

$$\frac{d\sigma(\epsilon)}{d\epsilon} = K\left(v, \frac{(x+U)^2}{2x+U}\right) \frac{-2x(x+U)}{(2x+U)^2}, \tag{23}$$

where $x = \epsilon - (m/2)v^2$ and $K(v,T) = d\sigma(v,T)/dT$.

The thin lines in Figure 10 show the cross-section for electron emission from a beam of neutral helium atoms interacting with a carbon target for a range of values of the velocity parameter ξ. The two electrons on helium are treated independently. With increasing ξ, i.e., increasing v, the binding energy U becomes less and less important, and hence the spectrum approaches a Dirac function around $mv^2/2$. Note the decrease in absolute magnitude with increasing projectile speed.

5.3 Projectile electron in orbital motion

Now consider a bound projectile electron moving with an orbital velocity $\boldsymbol{u}_e$. In the laboratory frame of reference $\mathcal{S}$, its velocity is $\boldsymbol{v}_e = \boldsymbol{v} + \boldsymbol{u}_e$. When this electron is scattered on a target atom at rest, its velocity becomes $\boldsymbol{v}'_e$ with $\boldsymbol{v}'_e \cdot \boldsymbol{v}_e = {v'_e}^2 \cos\theta$. Going back to the moving frame $\mathcal{S}'$, and taking into account the loss of ionization energy U, we get a change in speed but not in direction of motion.

The differential cross-section reads[2]

$$\frac{d\sigma(\epsilon)}{d\epsilon} = \left\langle \int d\sigma(v_e,\theta) \int_0^{2\pi} \frac{d\chi}{2\pi} \delta\left(\epsilon - \frac{m}{2} {v''_e}^2\right) \right\rangle_{\boldsymbol{u}_e}, \quad (24)$$

where χ is the azimuthal scattering angle.

After successive insertion, the electron energy ϵ reads

$$\epsilon = \frac{m}{2}v^2 - U + \frac{m}{2}\left(\boldsymbol{v}'_e - \boldsymbol{v}\right)^2 + m\boldsymbol{v}\cdot\left(\boldsymbol{v}'_e - \boldsymbol{v}\right)\sqrt{1 - \frac{2U}{m\left(\boldsymbol{v}'_e - \boldsymbol{v}\right)^2}}. \quad (25)$$

This is again evaluated in terms of spherical coordinates with $\boldsymbol{v}_e$ as the axis. However, dealing with a five-fold integration, of which only one is reasonably straightforward, the task to compute the differential cross-section is formidable. As a consequence, this new option in the PASS code requires computation times several orders of magnitude above all others: a spectrum of the type shown up till now requires a fraction of a second, while a spectrum of the present type requires an hour's CPU time on an efficient PC.

Figure 10 shows the He–C system studied both with and without orbital motion. A very drastic difference is observed. First of all, the narrow limits on the allowed velocity range are wiped out by the orbital motion. Secondly, the spectrum attains a pronounced peak at an energy slightly below $mv^2/2$. Thirdly, spectra level off only slowly toward velocity zero.

6 Multiple-shell systems

Multiple-shell systems are treated according to the Bohr scheme so that

$$\frac{d\sigma(\epsilon)}{d\epsilon} = \sum_j Zf_j \left(\frac{d\sigma(\epsilon)}{d\epsilon}\right)_j, \quad (26)$$

where Zf_j, the number of electrons in the jth shell, is determined from the spectrum of oscillator strengths f_j which satisfies the sum rule $\sum_j f_j = 1$.

6.1 Input

Equation (26) applies to both target and projectile. Typically, the index j refers to a principal shell for inner electrons and to a subshell for outer electrons. In the evaluations below, we have employed data for f_j, shell binding energies U_j and resonance frequencies ω_j compiled in reference [6]. Data used here have been listed in Table 1.

[2] Note the change in the velocity dependence of $d\sigma(v_e,\theta)$!

Table 1. Input parameters used in calculation of electron spectra. Data from [6].

Element	Z	Shell	Zf_j	$\hbar\omega_j$	U_j
He	2	$1s$	2.000	41.8	24.588
C	6	$1s$	1.992	486.2	288.2
		$2s$	1.841	60.95	16.59
		$2p$	2.167	23.43	11.26
Ne	10	$1s$	1.788	1525.9	869.5
		$2s$	2.028	234.9	47.7
		$2p$	6.184	56.18	21.564
Ni	28	$1s$	1.422	14346.9	8337.8
		$2sp$	7.81	1532.28	903.01
		$3sp$	8.385	262.71	84.88
		$3d$	8.216	74.37	10.213
		$4s$	2.167	23.03	7.6398
U	92	$1s$	1.047	180556.2	115606.0
		$2sp$	5.526	30088.1	19732.0
		$3spd$	15.709	6279.15	4162.13
		$4spdf$	32.730	1120.62	704.71
		$5spd$	18.066	127.44	164.15
		$6sp$	8.542	48.08	27.325
		$7s$	2.028	38.19	6.1941
		$6d$	3.238	36.5	6.1
		$5f$	5.114	32.94	6.

6.2 An example

Figure 11 shows spectra for the He^0–C system for a range of ξ-values, with and without projectile excitation included. It is seen that projectile excitation constitutes an important contribution mainly in the region around $\epsilon \simeq mv^2/2$. The process of electron capture to continuum (ECC) regime is commonly assumed in the literature to contribute to this spectral regime [3]. The process treated here, however, comes close to electron loss into the continuum. Indeed, the interaction cross-section for collisions between a neutral target atom and a projectile electron has its maximum for soft collisions in the moving system, i.e., where the final speed of the projectile electron will not be far away from the beam speed v, except for low values of ξ, where the orbital electron motion dominates.

6.3 Scaling law?

We wish to explore the possibility that electron spectra also in the multishell case obey the Bohr scaling relation. To this end we first consider data for target excitation only (Fig. 12). For the scaling variable $t = (\epsilon + U)\xi^2/2mv^2$ we need quantities ω and U for a multishell system. For ω we employ the common definition from the Bethe theory,

$$\ln\omega = \sum_j f_j \ln\omega_j, \quad (27)$$

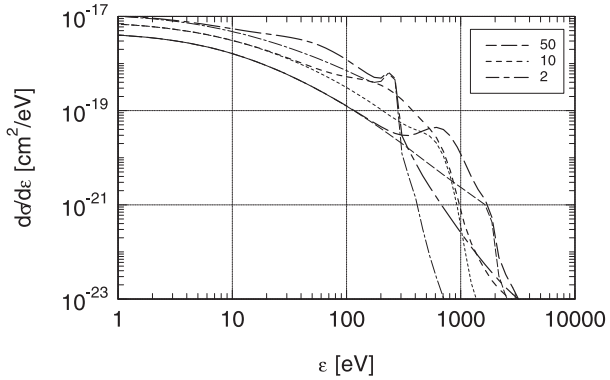

Fig. 11. Electron spectra for He^0 on C for $\xi = 2, 10, 50$. Thick lines: target and projectile ionization. Thin lines: target excitation only. Orbital motion included in all cases.

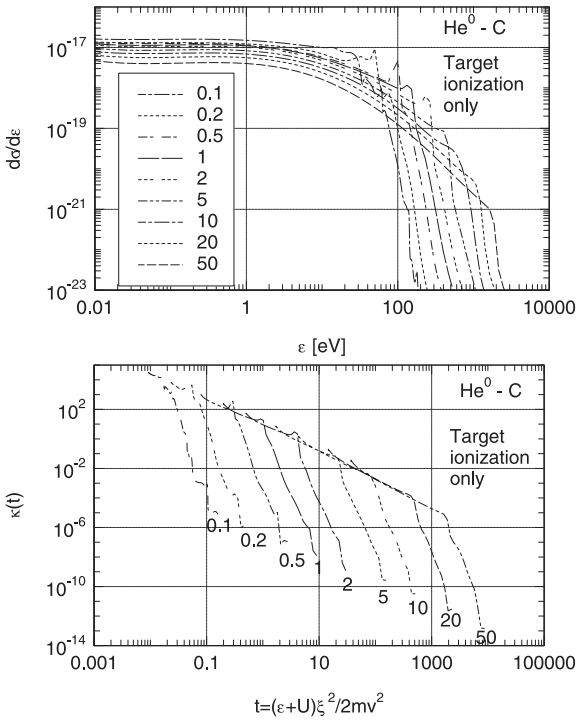

Fig. 12. Electron spectra for He^0–C as in Figure 11. Target excitation only. Upper graph: absolute units. Lower graph: dimensionless units. Both plots show the differential cross-section *per target atom.*

and for U, we use the analogous expression,

$$\ln U = \sum_j f_j \ln U_j. \tag{28}$$

The lower graph in Figure 12 shows the result. It is seen that apart from a region around the cutoff, the soft-interaction portion satisfies Bohr scaling very well. Note that for an absolute comparison with similar graphs such as Figure 1 the curves would have to be divided by 6, the number of electrons per carbon atom.

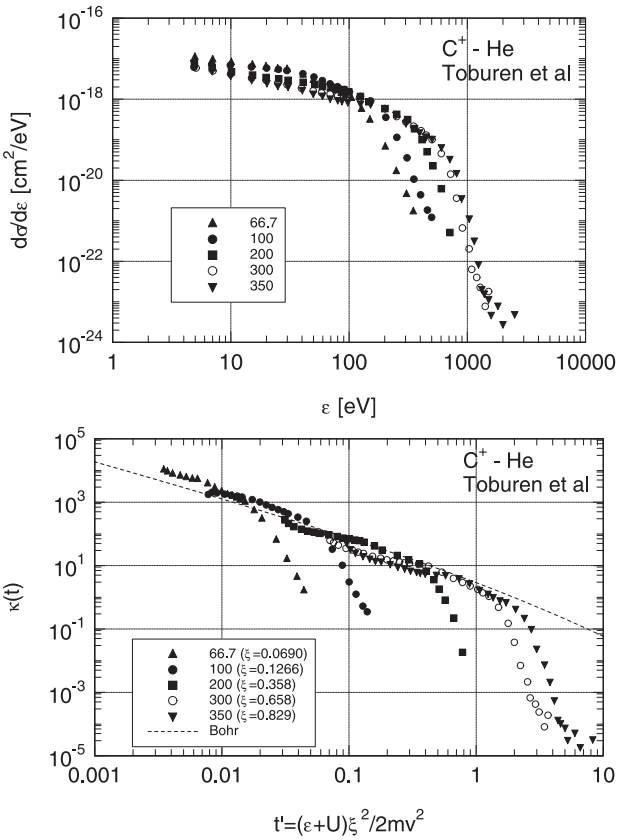

Fig. 13. Experimental spectra for C^+–He from [28] in absolute (upper graph) and dimensionless (lower graph) units. Labels indicate the beam energy in keV/u.

The two Figures 13 show a similar comparison, but now employing experimental data for the C^+–He system at five different beam speeds. Experimental data include projectile processes which do not obey Bohr scaling in the form obeyed by target spectra. Hence, deviations from simple Bohr scaling must be expected. This is indeed found, and from Figure 11 it is not surprising that deviations reach up to a factor of two. Nevertheless, the assumption of Bohr scaling may be useful starting point in establishing rough expressions for electron spectra where measurements and detailed calculations are unavailable.

6.4 Comparison with experiment

Figure 14 shows a comparison of our absolute estimates with measurements of Toburen et al. [28] on the C^+–He system. Also included are CTMC-calculations from reference [28]. Generally good agreement is found between our calculations and the measurements in the region around the cutoff. One could argue that this regime is the domain of the classical binary-encounter theory. However, projectile screening is an essential feature here, as is projectile excitation at slightly smaller electron energies. Agreement is reasonable also in the soft-collision regime, although in almost all cases, the CTMC approach does slightly better. We presume that this indicates the presence of collective

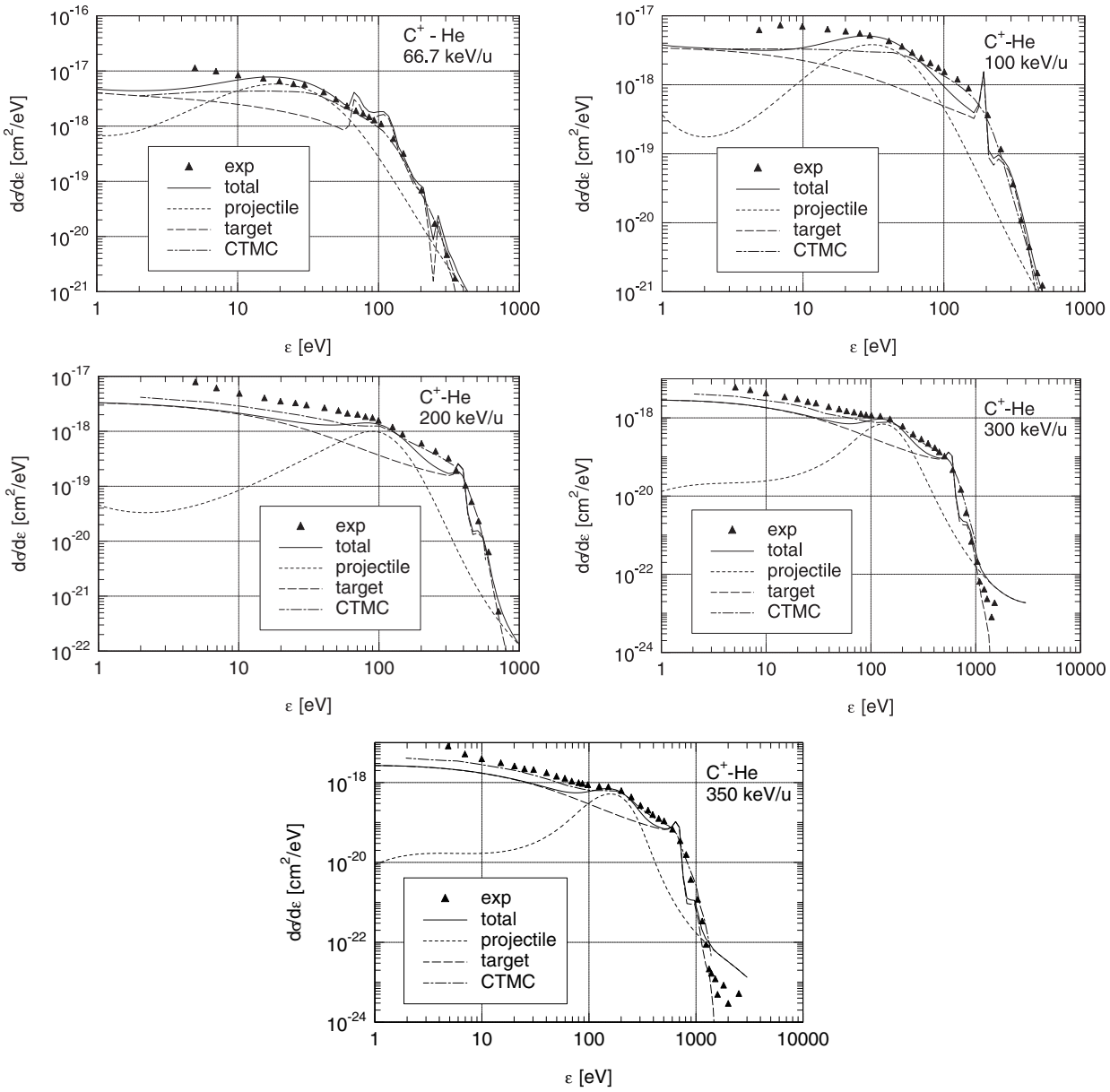

Fig. 14. Comparison of measured with calculated spectra for C^+–He. Experimental data from [28]. Calculations by binary theory involving orbital motion of both target and projectile electrons. Calculations by classical-trajectory Monte Carlo quoted from [28].

processes that are not allowed for in our description but which are well-known to be visible in CTMC calculations.

Similar conclusions emerge from Figures 15 and 16 for the Ni–He and U–Ne system, respectively.

7 Note on ionization cross-sections

Except for the behavior near threshold, the total ionization cross-section is determined primarily by fairly soft collision events for which Bohr and Bethe theory predict equivalent results. While the present work suggests scaling relations that do not seem to have been explored, we nevertheless consider this topic somewhat outside the mainline of this paper.

However, little opportunity has been given to check the validity of our charge-state model. Therefore, we include two graphs showing a comparison between measured and calculated ionization cross-sections in their dependence on the ionic charge state.

Figure 17 shows a comparison between calculated and measured ionization cross-sections for 1 MeV/u F on Ne and Ar. Electrons emitted from the target and from the projectile are considered separately both in the calculations from binary theory (including orbital motion) and in the experimental data (where charge states of recoils and ions were analysed). Good agreement is found in both

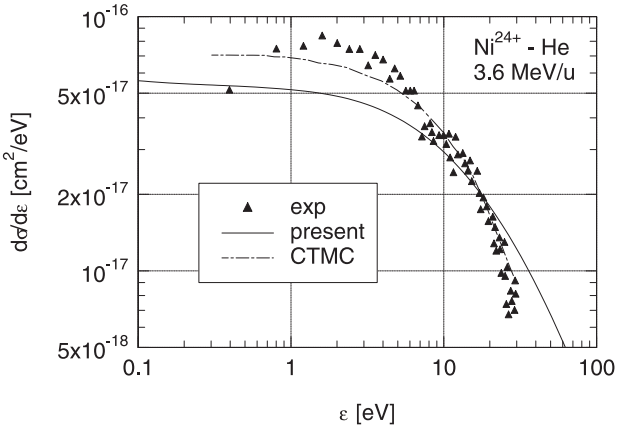

Fig. 15. Comparison of measured with calculated spectra for Ni^{24+}–He. Experimental data from [29]. Calculations by binary theory of total, projectile and target electron emission including orbital motion. Calculations by classical-trajectory Monte Carlo quoted in the original paper.

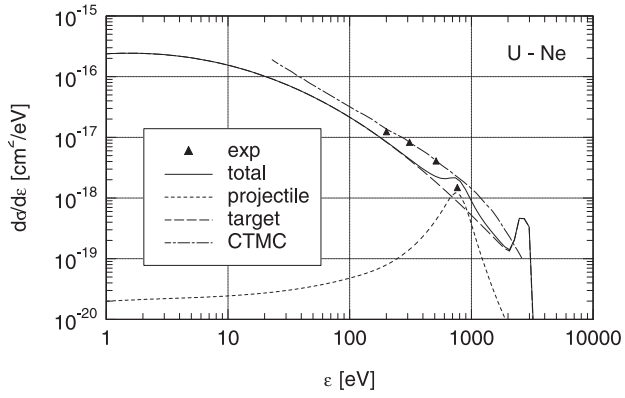

Fig. 16. Comparison of measured with calculated spectra for U^{32+}–Ne. Experimental data from [30]. Calculations by binary theory of total, projectile and target electron emission including orbital motion. Calculations by classical-trajectory Monte Carlo quoted in the original paper.

cases, except for low charge states where the theory tends to overestimate measured ionization cross-sections. This indicates that screening is more complete than what is predicted from our description. We plan to follow up this point further by looking in detail at the large amount of pertinent experimental data that are available in the literature.

8 Discussion

General considerations as well as examples discussed in this paper refer to the 'classical regime', i.e., experimental conditions where $\kappa_{\rm Bohr} = 2Z_1 v_0/v > 1$. While we have no reason to doubt that there is a smooth transition to the Born regime, we have not studied this aspect here[3].

[3] but have done so in great detail in connection with stopping phenomena, cf. [32].

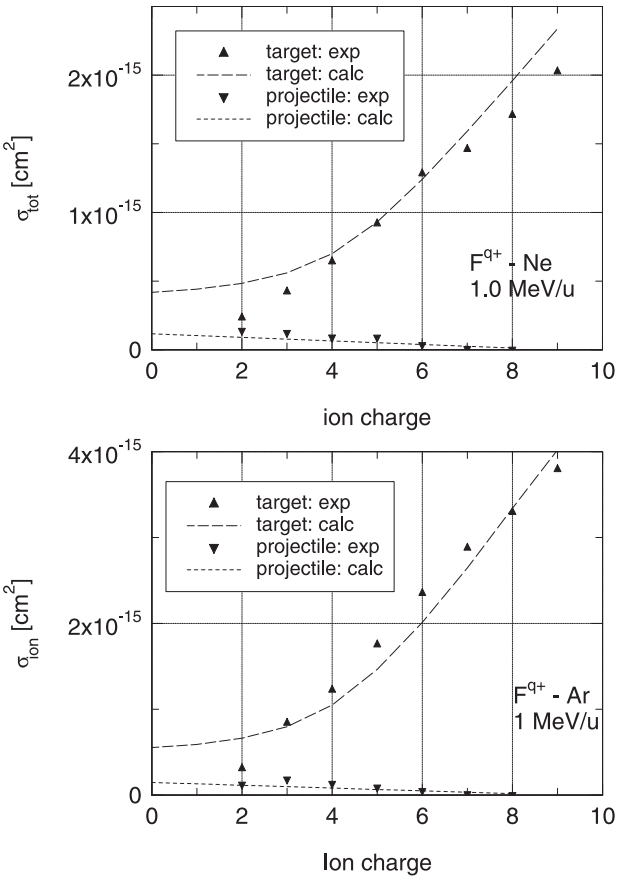

Fig. 17. Total ionization cross-section calculated from binary theory versus ionic charge state, compared to experimental data from [31]. Upper graph: 1 MeV/u F–Ne; lower graph: 1 MeV/u F–Ar.

Two conventional tools are available for the analysis of electron spectra in the classical regime in addition to straight Coulomb scattering: binary-encounter theory and classical-trajectory simulation (CTMC). Comparing the present scheme with the binary-encounter model, both allow for orbital motion, but unlike Bohr theory, the binary-encounter model ignores all influence of binding on the collision dynamics. This weakness does not apply to the CTMC model which, however, has the weakness of lacking transparency as any large-scale computational procedure. In particular, there is no obvious way to extract scaling relations of the type uncovered here from a CTMC simulation code.

Our model utilizes a well-defined charge-state model which, however, may have to be modified if a more detailed study of ionization cross-sections should confirm the trends emerging from Figure 17.

Electrons emitted from the target and the projectile are calculated in separate procedures, and systems have been studied where projectile electrons can by no means be neglected. In the present version of our PASS code, projectile electrons require several orders of magnitude longer computation times than target electrons. This is one reason for our scheme to be considered more promising for

systems where $Z_1 < Z_2$, for which target electrons tend to dominate. Another reason is the fact that the scaling law expressed by Figure 1 may be optimally fulfilled for such systems, cf. Figure 9.

An important distinction between binary stopping theory and Bohr theory is the incorporation of the Barkas-Andersen effect in the former, i.e., the presence of uneven terms in Z_1. This difference also prevails in electron spectra, but it is much less dramatic, because it concerns mainly a fairly narrow interval of electron energies ϵ not far from the maximum. We note, however, that for many years it used to be a widespread belief that the Barkas-Andersen effect in stopping was a phenomenon restricted to fairly large impact parameters [33].

While we tend to consider the scaling relations discussed in this paper as being more relevant and, presumably, also more well-founded than the details of our quantitative model, we have performed explicit comparisons with measurements which, by and large, lead to results that confirm the essentials of the theoretical model.

This work has been supported by the Danish Natural Science Research Council (FNU).

References

1. N. Bohr, Mat. Fys. Medd. Dan. Vid. Selsk. **18**, 1 (1948)
2. ICRU, *Secondary electron spectra from charged particle interactions*, Vol. 55 of ICRU Report (International Commission of Radiation Units and Measurements, Bethesda, Maryland, 1996)
3. N. Stolterfoht, R.D. DuBois, R.D. Rivarola, *Electron emission in heavy ion-atom collisions*, Springer Series on Atoms and Plasmas (Springer, Berlin, 1997)
4. ICRU, *Stopping powers and ranges for protons and alpha particles*, Vol. 49 of ICRU Report (International Commission of Radiation Units and Measurements, Bethesda, Maryland, 1993)
5. P. Sigmund, *Stopping of heavy ions*, Vol. 204 of Springer Tracts of Modern Physics (Springer, Berlin, 2004)
6. ICRU, *Stopping of ions heavier than helium*, Vol. 73 of ICRU Report (Oxford University Press, Oxford, 2005)
7. H. Bethe, Ann. Phys. **5**, 324 (1930)
8. N. Bohr, Philos. Mag. **25**, 10 (1913)
9. P. Sigmund, Phys. Rev. A **54**, 3113 (1996)
10. P. Sigmund, Phys. Rev. A **56**, 3781 (1997)
11. F. Bloch, Ann. Phys. **16**, 285 (1933)
12. J. Lindhard, A.H. Sørensen, Phys. Rev. A **53**, 2443 (1996)
13. J.H. Macek, Nucl. Instrum. Meth. B **53**, 416 (1991)
14. P. Sigmund, A. Schinner, Eur. Phys. J. D **12**, 425 (2000)
15. P. Sigmund, A. Schinner, Nucl. Instrum. Meth. B **195**, 64 (2002)
16. M.S. Weng, Master's thesis, University of Southern Denmark (2002)
17. M.S. Weng, A. Sharma, P. Sigmund, A. Schinner (2004), poster presented at ICACS-21, Internat. Conf. Atomic Collisions in Solids, Genova, Italy
18. W. Brandt, M. Kitagawa, Phys. Rev. B **25**, 5631 (1982)
19. J. Lindhard, Nucl. Instrum. Meth. **132**, 1 (1976)
20. P. Sigmund, A. Schinner, Eur. Phys. J. D **15**, 165 (2001)
21. M.M. Basko, Eur. Phys. J. D **32**, 9 (2005)
22. P. Sigmund, A. Schinner, Phys. Rev. Lett. **86**, 1486 (2001)
23. R.E. Olson, C.O. Reinhold, D.R. Schultz, J. Phys. B **23**, L455 (1990)
24. P. Sigmund, Phys. Rev. A **26**, 2497 (1982)
25. A.L. Tofterup, J. Phys. B **16**, 2997 (1983)
26. E. Gerjuoy, Phys. Rev. **148**, 54 (1966)
27. P. Sigmund, A. Schinner, Nucl. Instrum. Meth. B **243**, 457 (2006)
28. L.H. Toburen, R.D. Dubois, C.O. Reinhold, D.R. Schultz, R.E. Olson, Phys. Rev. A **42**, 5338 (1990)
29. R. Moshammer, J. Ullrich, M. Unverzagt, W. Schmidt, P. Jardin, R.E. Olson, R. Mann, R. Dorner, V. Mergel, U. Buck et al., Phys. Rev. Lett. **73**, 3371 (1994)
30. R. Olson, J. Ullrich, H. Schmidt-Boecking, Phys. Rev. A **39**, 5572 (1989)
31. O. Heber, G. Sampoll, B.B. Bandong, R.J. Maurer, R.L. Watson, I. Benitzhak, J.M. Sanders, J.L. Shinpaugh, P. Richard, Phys. Rev. A **52**, 4578 (1995)
32. P. Sigmund, *Particle penetration and radiation effects*, Vol. 151 of Springer Series in Solid-State Sciences (Springer, Berlin, 2006)
33. J.C. Ashley, R.H. Ritchie, W. Brandt, Phys. Rev. B **5**, 2393 (1972)